A Cryogenic Integral Field Spectrograph for the Palomar 200-inch Telescope

T. W. Murphy, Jr., K. Matthews, and B. T. Soifer
Palomar Observatory, California Institute of Technology, 320-47, Pasadena, CA 91125
Electronic Mail: tmurphy@mop.caltech.edu; kym@caltech.edu; bts@mop.caltech.edu

ABSTRACT

We present the design, construction, and performance of a near-infrared integral field spectrograph now in operation at the Palomar Observatory 200-inch Telescope. The spectrograph acts as a front-end to one of two existing infrared cameras, covering the 1–2.5μm and 1–5μm wavelength ranges. An all-aluminum image slicer splits the $5.4'' \times 9.6''$ field of view into eight slits, feeding two independent spectrographs within the same dewar. Spectra are simultaneously obtained for all points within the field, with seeing-limited spatial resolution. Two resolution modes of $R \approx 1300$ and $R \approx 600$ are available, as well as a broad-band imaging mode for photometry and target acquisition. The spectrograph was first operated on the 200-inch Telescope in 1998 September. Performance has been as predicted, with a total system throughput of $\sim$22% from the top of the atmosphere to electron counts. Sensitivity is estimated to allow detection of a $K = 18$ mag (0.04mJy) continuum point source at the 5σ level in one hour of integration at the high resolution setting. Example data from the spectrograph are presented here.

Subject headings: instrumentation: spectrographs—galaxies: interactions—infrared: galaxies—galaxies: individual (NGC 6240, 4C 39.37)—radio continuum: galaxies

1. Introduction

The introduction of large-format infrared arrays in the early 1990s made possible the development of imaging systems with moderate fields of view and spectrographs with good spectral coverage at moderate resolutions. The large arrays also permit the implementation of integral field spectroscopy, wherein spectral information is simultaneously gathered for all points in a two-dimensional field, and recorded on the two-dimensional array. A single integration thus results in a datacube, with two spatial axes and one spectral axis. This technique was first exploited in the near-infrared by Weitzel et al. (1996), with an instrument called 3D.

The advantages of integral field spectroscopy in generating three-dimensional datacubes go beyond the efficiency aspect of gathering multiple adjacent longslit spectra simultaneously (see Weitzel et al.,1996). The simultaneity itself results in observations that are insensitive to problems associated with variable atmospheric conditions, such as seeing and photometry. Unlike sequentially generated datacubes obtained by either stepping a longslit across the object, or tuning a Fabry-Perot imager to a sequence of wavelength settings, the integral field technique is not affected by lack of precision in telescope pointing or etalon tuning. The simultaneous coverage of continuum and line emission in two dimensions allows subtle offsets and morphological differences to be elucidated. An additional advantage over longslit spectroscopy is that all the flux from the observed object is represented on the array, rather than some portion being lost at the slit. Integral field spectroscopy is particularly useful for observations of morphologically complex objects, especially those with structure in the velocity domain as well.

The Palomar Integral Field Spectrograph (PIFS) was designed primarily for the study of ultraluminous infrared galaxies, though it is also well suited for observations of high-redshift radio galaxies, circumnuclear environments of Seyferts, and quasar host environments.

2. Instrument Design

The Palomar Integral Field Spectrograph (PIFS) operates at the tip-tilt corrected $f/70$ focus of the Palomar 200-inch Telescope. It is designed to present an $f/70$ output focal plane to one of two existing infrared imaging cameras. The primary design camera employs a 256×256 HgCdTe (NICMOS 3) array, which operates from 1–2.5μm. Also available is a 256×256 InSb array camera, permitting operations out to 5μm. The approach of having separate dewars for spectrograph and camera, while introducing extra optical elements—and more significantly, a warm window interface—was taken to facilitate a rapid and inexpensive instrument project. The technique has been successfully implemented in the Palomar Longslit Infrared Spectrograph (PLIS) (Larkin et al. 1996), upon which the PIFS design is based. For simplicity, the PIFS design was tailored to fit within the PLIS dewar envelope. This constraint guided the overall size and appearance of the spectrograph, though ultimately the PIFS was housed in its own dewar.

2.1. The Image Slicer

A cryogenic image slicer is used to rearrange the two-dimensional focal plane into effectively a long slit. This effective long slit is actually made of smaller sub-slits, which are sliced out of the focal plane. By mapping the two-dimensional focal plane into a pseudo-one-dimensional arrangement, one can disperse light in the cross-slit direction to effectively obtain a spectrum at each position in the two-dimensional field without convolving spatial and spectral information. Figure 1 illustrates this concept.

The use of existing cameras to record the spectral image imposes a predetermined pixel scale of 0.167 arcsecond pixel^{-1} for the HgCdTe array camera, which is the assumed camera in all that follows. The total unvignetted field of view of the camera is just under 40$''$ across. With a slit width of 0$''$.67 (4 pixels), the total area of a longslit spanning the array is about 25 arcsecond^2. In order to double the total field of view, the image slicer is designed to produce two effective longslit outputs, as depicted in Figure 1. In doing this, only half the array is available for spectral dispersion of each slit, sacrificing spectral coverage per slit in favor of increased field of view. While a slit width of 0$''$.33 (2 pixels) would have produced a critically sampled spectral output, the effective field area would be half that attainable with a 4-pixel wide slit. For the PIFS science drivers, field of view is more important than spectral coverage. The final design of the image slicer therefore has a total field of view of $\sim$50 arcsecond^2, slicing this field with 0$''$.67 wide slits, corresponding to a 4 pixel width on the HgCdTe array camera.

A rectangular field pattern is chosen to provide observational flexibility, and to simplify the image slicer design by reducing the number of sub-slits needed. The 5$''$.4×9$''$.6 field of view can be rotated to any position angle on the sky by rotating the Cassegrain instrument mount about the telescope optical axis.

The image slicer is constructed entirely out of aluminum alloy #6061-T651. The optical elements have diamond fly-cut reflective surfaces coated with protected silver. The first set of image slicer optics are eight

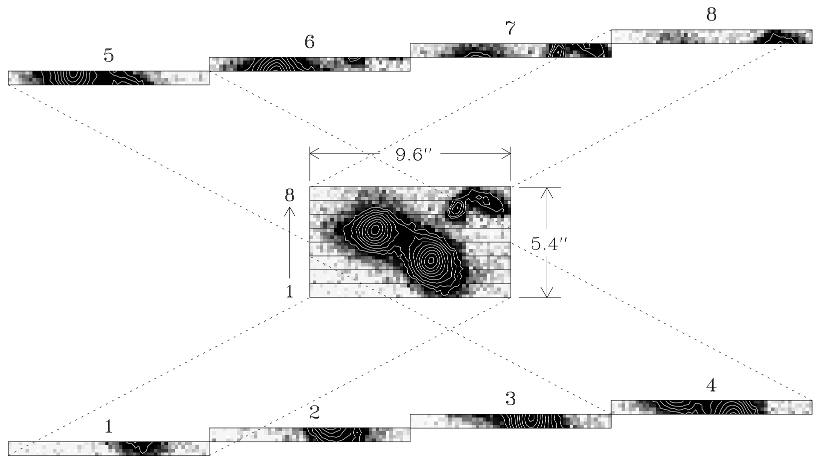

Fig. 1.— Schematic representation of the image slicing concept. The rectangular field is sliced into eight strips, or sub-slits, which are rearranged in an end-to-end configuration such that light from each slit may be dispersed without overlapping. The PIFS image slicer produces two effective long slits, for reasons described in the text.

planar facets each measuring 1.17mm$\times$17.8mm in size. These facets sit at the $f/70$ focal plane, directing the incident light into eight different directions. Sitting roughly 100mm away from the focal plane are a second set of planar facets, these being 2.92mm$\times$17.2mm in size. Upon reaching these mirrors, the eight slits have separated into two groups of end-to-end patterns, as depicted in Figure 1. Each of the second set of mirrors intercepts the light from one of the flat mirrors in the focal plane and sends it toward the spectrograph as if originating from a common pupil at the distance of the telescope secondary mirror. Figure 2 depicts the physical arrangement of the end-polished optical elements in the image slicer, and shows the optical paths through the system.

Producing an image slicer with eight separate optical paths yet preserving the $f/70$ pupil to a few percent of the pupil diameter requires angular alignment of each mirror to $\sim$0.1 milliradian. This alignment must be maintained in the cryogenic environment. The technique for fabricating the image slicer optics is such that random alignment errors were minimized. The image slicer optics are then mounted onto a monolithic aluminum fixture, which helps to control random alignment error and provides a homogeneous material environment such that thermal contraction is the same for both fixture and optics.

Each slicer optical element is a thin plate roughly 17mm$\times$60mm in size, with a flat optical surface on one end. Each plate has a common set of two pinholes establishing the final position and alignment of the optic on the mounting fixture. One of these holes is centered on each plate near the front—or reflecting—end of the optic. The second pinhole is at the back end, in one corner of each plate. A third pinhole at the back end of the plate, in combination with the front, or pivot, pinhole establishes an alternate configuration such that the line between these two pinholes is perpendicular to the optical surface. When all the plates are stacked together with a pair of pins running through this alternate set of pinholes, a single, coplanar surface is presented. A flat surface is diamond fly-cut on the end of this stack to simultaneously produce all of the optical surfaces. The final configuration, established by the pivot pinhole and the common corner pinhole, will then fan the reflecting surfaces out in a variety of angles. The relative angle between surfaces is solely

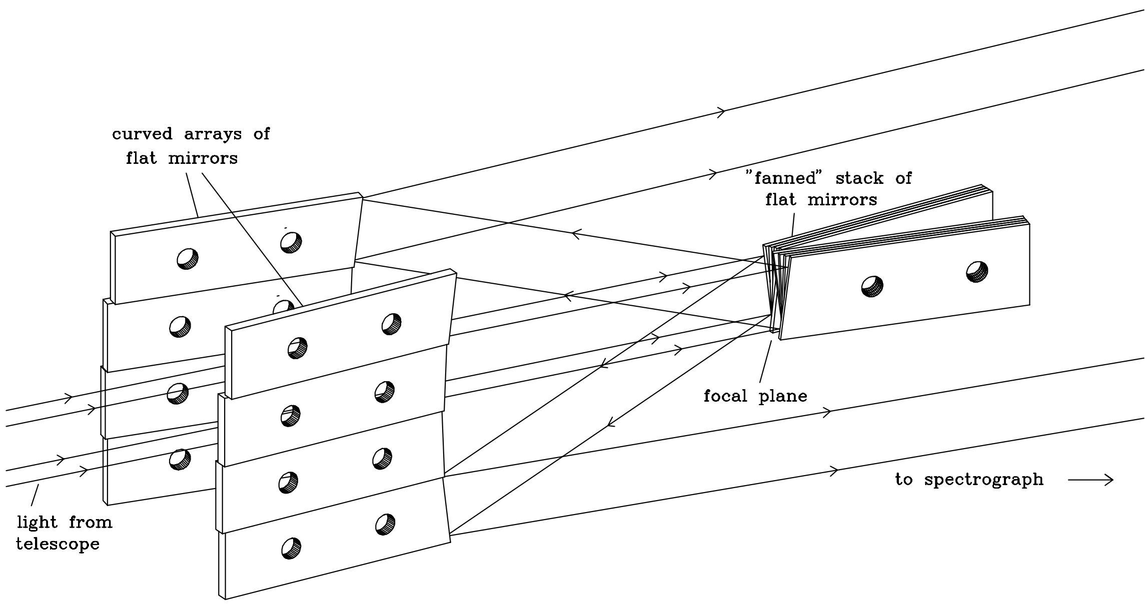

Fig. 2.— Arrangement of image slicer optical elements. The optical elements are aluminum plates, diamond fly-cut on the ends to form optically flat reflective surfaces. The stack of thin mirrors at the focal plane redirects the field onto eight collector mirrors, at left, which send the light towards the spectrograph in the end-to-end pattern depicted in Figure 1. The four rays shown illustrate the optical paths for the two outermost slits in the focal plane.

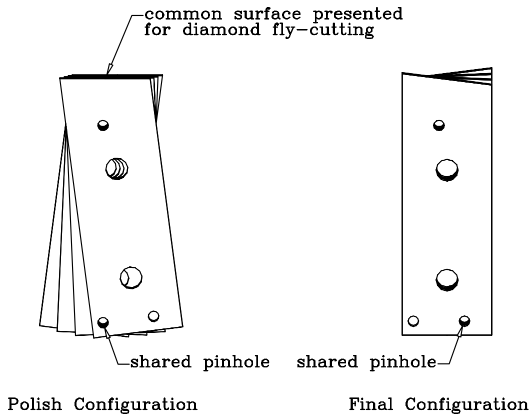

Fig. 3.— The image slicer optics were diamond fly-cut simultaneously in the stack configuration illustrated at left. The final configuration, with a variety of reflector orientations, is shown at right. Precision pinholes used in the fly-cut and final configurations completely determine the relative angles of the reflective surfaces. See text for details.

determined by the angle between the three pinholes in any given plate. Thus controlling alignment to $\sim$0.1 milliradian with pinholes separated by $\sim$50mm requires a pinhole positional accuracy of 5μm, which is within the reach of an accurate milling machine. Figure 3 illustrates the principle involved.

The figure accuracy of the thin focal plane optical elements is measured to be flat to $\sim$200nm, peak-to-valley, while the thicker, more robust second set of elements has a peak-to-valley figure accuracy of $\sim$60nm.

The actual slit pattern produced by the image slicer is not the regular stair-stepped pattern illustrated in Figure 1. Because the image slicer optics are tilted about two axes, which is necessary to separate the two long slits, the image slicer focal plane elements are capable of casting shadows on adjacent elements. The actual order of the slits is rearranged to move the focal plane shadows out to the corners of the field rather than have them near the field center. This is accomplished by selecting the high-angle slices, corresponding to the ends of the long slit, to represent the outer slits in the integral field, thus using the low angle slices for the central part of the field. As a result, the actual longslit pattern, rather than being ordered 1-2-3-4 as shown in Figure 1, is ordered 1-4-3-2. This pattern is evident in the raw spectra, seen in Figure 5. Note that the arrangement of optical elements in Figures 2 and 3 would produce the regular stair-stepped pattern of Figure 1, and therefore do not represent the actual arrangement of the PIFS image slicer optical elements.

2.2. The Spectrograph

The PIFS optical layout is shown in Figure 4. Because the image slicer delivers two effective longslits, and because the spectra from each of these must not overlap, two identical spectrographs are housed within the same dewar, one for each of these effective slits. Tunable narrow band interference filters offer another potential solution for separating the two spectra. However, the large range of angles passing through the filter location in the infrared cameras used here result in a lack of uniform spectral coverage across the array. Therefore the separation of spectra is accomplished by physically separating optical paths.

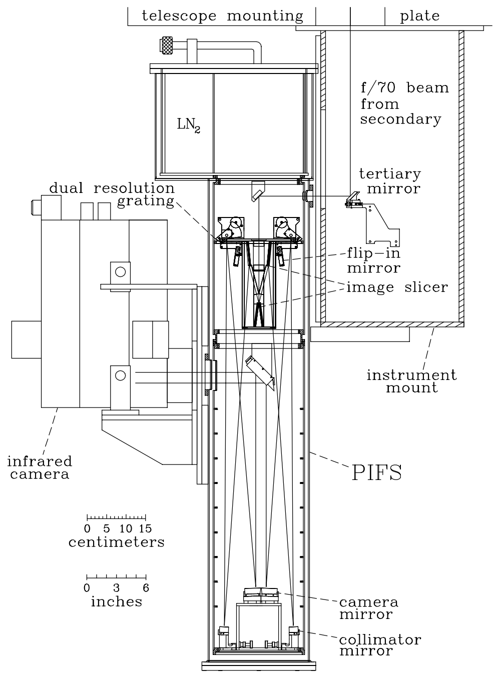

Fig. 4.— The PIFS dewar and optical path. The infrared camera is a separate dewar attached to the PIFS dewar at left.

Referring to Figure 4, the $f/70$ beam from the telescope reflects off the tertiary fold mirror and into the cryogenic environment through an anti-reflection coated sapphire window. Another fold mirror directs the beam to a focus at the image slicer. The action of the image slicer is described in section 2.1. Following one of the two effective slits from the image slicer, the beam goes to one of the two identical spectrographs. A 940mm focal length spherical collimator places an image of the 13mm pupil on the grating surface. A mirror can be rotated in front of the grating to produce an image of the slit rather than a spectrum. Because this is a separate mechanism, the grating position is not disturbed during this operation, allowing one to switch between imaging mode and spectral mode without affecting grating reproducibility. For each spectrograph there are two aluminum-coated epoxy replicas affixed to a single aluminum substrate. One of the grating surfaces has a blaze angle of 36.°8 and 300 grooves per mm, providing a spectral resolution of $R \equiv \lambda/\Delta\lambda \approx 1300$. The grating may be rotated via stepper motors in steps of 0.2 milliradians for wavelength selection. Rotating the grating block through $\sim 50°$ moves the second replicated grating surface into the beam, with a blaze angle of 17.°5 and 150 grooves per mm for $R \approx 600$ spectra. From the grating, the beam travels to another spherical mirror, identical in focal length to the collimator mirror. An $f/70$ converging beam is produced, and merging with the beam from the twin spectrograph, is deflected off a fold mirror, exiting through the CaF_2 dewar window en route to the infrared camera. All mirrors except those in the image slicer are overcoated gold on fused silica substrate. Raytracing of the integrated system produces a spot size of <0.05 arcsecond at the camera focal plane.

Order sorting is accomplished via filters within the infrared camera. A 5% circular variable filter (CVF) performs this function for the wavelength range of 1.5–2.5μm, and broadband filters are used for wavelengths outside of this range. Each spectrum spans ∼25 resolution elements on the array, corresponding to ∼5000 km s^{-1} in high resolution mode, and $\sim$12000 km s^{-1} in low resolution mode. The spectral coverage in low resolution mode is sufficient for simultaneous acquisition of line pairs such as H_2 1–0 S(1) + Brγ, [Fe II] + Paβ, and even [O III] + Hβ in high redshift sources.

Spectral calibration is provided in part by the OH airglow emission where available. Emission lines from neon, argon, krypton, and xenon arc lamps are used to supplement or substitute for the OH lines. Any combination of lamps may be turned on at once, the light from which strikes a retractable sandblasted surface roughly at the position of the tertiary mirror.

The gratings and the flip-in mirrors used for imaging are rotated by stepper motors external to the dewar. Motor driven shafting is fed through a series of o-rings and spacers, bracketed by ball bearings. Following each feed-through is a flexible coupling, a fiberglass shaft, a shaft coupling, a wafer spring coupling, a fixed bearing, and a bi-directional clutch. The flip-in mirrors are direct-drive, while the gratings move through a double gear reduction with a total reduction of about 1:78. Torsion springs force the flip-in mirrors against their mechanical stops, and coiled constant-force springs attached to the gratings load the grating gear trains. Grating reproducibility has been measured at better than 0.2 pixels, or $\sim$0.05 milliradians.

The spectrograph, including the image slicer, is cooled by liquid nitrogen to a temperature below $\sim 80^\circ$K in an effort to minimize dilution of the astronomical signal by thermal emission from the optical surfaces and surrounding supports. This is particularly beneficial for preventing stray light from mixing into the many beams of the image slicer, which is virtually impossible to baffle. The liquid nitrogen is held in a cylinder at the top of the instrument, as seen in Figure 4. The dewar has a capacity of 22 liters, with a hold time of approximately three days.

The PIFS optical path is heavily baffled, with eight baffle fins between the entrance window and the image slicer focal plane, and eleven baffle planes located between the optics at the top end of the dewar and the optics at the bottom. Considering the multiple passes, a single photon traverses 48 baffle plates while inside the PIFS dewar. Most internal surfaces of the PIFS dewar are coated with Aeroglaze WZ306 flat black polyurethane coating. In addition to these stray light controls, the mechanical couplings to the outside stepper motors, which are partially isolated by a fiberglass shaft connection, are surrounded by cold baffle material, such that no direct light path exists from the warm outside environment to the optical train without first intercepting a cold surface. An additional baffle box surrounds the grating assembly, further reducing stray light from the vicinity of the grating. The infrared camera contains similar baffling systems, in addition to a cold Lyot stop to filter out unwanted light at the pupil.

The imaging camera is situated in a gimbal with two translational degrees of freedom and two rotational degrees of freedom allowing for proper positioning of the focal plane and alignment of the PIFS pupil to the camera's cold stop. Alignment of the PIFS dewar to the telescope pupil is accomplished via an adjustable tertiary mirror, which sits on a sliding stage within the warm instrument mount.

Internal spectrograph alignments are all accomplished via motions of the spherical mirrors at the base of the dewar. The alignment can only be performed when the dewar is warm and the vacuum vessel open to the atmosphere. The all aluminum construction nullifies differential contraction such that alignment is maintained in the cold state. Because the alignment involves spherical mirrors, translational motions are equivalent to rotations. Each mirror has two-dimensional fine-adjust motion capability for the purpose of alignment. Co-alignment of the twin spectrographs is critical, since each independent spectrograph pupil must fall on the same cold stop in the camera.

The measured efficiency of the PIFS-camera system in high resolution spectral mode is $\sim$22% from the top of the atmosphere to detected photons, assuming an 80% combined transmission of the the atmosphere and telescope. The PIFS dewar itself has a throughput of $\sim$58% with the grating on blaze. The dominant loss in the system is due to the grating. The image slicer throughput, including pupil losses, is 90–95%. An additional source of loss for the entire system is a pair of CaF_2 windows separating the camera dewar from the PIFS dewar. The combined transmission of this pair of windows is about 85%. Estimates of sensitivity indicate the ability to detect a $K = 18$ mag continuum point source (0.04 mJy) at 5σ in one hour of on-source integration under good seeing conditions.

The entire optical assembly is cantilevered off the bottom plate of the nitrogen tank. A perforated tube internal to the nitrogen canister acts as an extension of the optical tube, adding structural rigidity to the assembly by connecting the top and bottom plates of the nitrogen canister together. Flexure of the assembly, as measured via lamp line spectral positions at the camera focal plane, is never more than one-half pixel for any motion of the telescope above an elevation of 25°.

3. Observation Techniques

Observing with the PIFS is a straightforward process, typically involving alternating object and sky integrations. If the observed object is only a few arcseconds in extent, as is often the case for high-redshift radio galaxies, for instance, the object can be dithered around within the PIFS field such that all integration time is spent on the object. The disadvantage to acquiring separate sky frames is that the OH airglow lines are time variable on the scale of minutes. However, the spatially uniform, spectrally discreet nature of these lines makes removal of residual flux feasible in software.

The imaging mode, with the flip-in mirror placed in front of the grating, produces a sliced image of the field of view. Though not difficult to mentally reconstruct, quick-look software enables immediate reassembly of the field into its original rectangular form. The imaging mode is used to acquire and center observing targets within the field. Unlike longslit spectroscopy, integral field spectroscopy does not require precise positioning within a slit, thereby simplifying the process of target acquisition. The imaging mode is also useful for photometric calibration with broad-band photometric standards, though the spectral modes may also be used for photometric calibration.

Any image slicing spectrograph having little anamorphic magnification and a pixel scale that does not greatly oversample the seeing has an inherent sampling asymmetry in the following way. If the slits correspond to one pixel in width, thereby symmetrically sampling spatial data in both the cross-slit and along-slit directions, the spectral output is undersampled, with unresolved spectral sources spanning only one pixel in the spectral direction. For critically sampled spectral data, the slit must be two pixels in width, which imposes a cruder spatial sampling in the cross-slit direction as compared to the along-slit direction. For the PIFS, with 4-pixel wide slits (see section 2.1 for details), the problem is even more exaggerated. The spatial sampling of a single PIFS exposure is sufficient to resolve $0\farcs33$ structures in the along-slit direction, but sampling in the cross-slit direction limits resolution to a crude $1\farcs33$. To compensate for this asymmetry, an appropriate dither pattern can, in stable seeing conditions, allow one to recover the full spatial resolutions in both dimensions. In practice, this has worked quite well, as can be seen in the example data shown in section 5.

Atmospheric opacity as a function of wavelength is measured just prior to or just after the object observation by observing a featureless stellar spectrum at similar airmass and direction in the sky.

Main-sequence G-stars with $V < 6.5$ mag are used for this purpose. Within the near-infrared bands, these stars very nearly approximate blackbodies with only minor absorption features at Paβ and Brγ, which are easily interpolated over.

Flat fielding is accomplished simultaneously with spectral calibration observations of the G-star, by uniformly illuminating the PIFS field with the light of the star. In practice this is done by chopping the $f/70$ secondary mirror in a triangle-wave pattern, in a direction coinciding with the PIFS slit direction. By guiding on the endpoint of the chopped star with a moving autoguider head, the star is steadily dragged across all the slits, with a double-pass taking roughly 180 seconds. Thus the object-sky pair is obtained in $\sim$400 seconds. Telescope shake, seeing variability, etc., can unevenly distribute light among the slits, so a second spectrum is taken, this time with the star chopped across the slits, rather than along them. A brief exposure provides a relative flux reference, as it is known that each slit receives the same amount of light. In addition, this exposure establishes a spatial reference with which to tie the spectral observations together. This complicated technique is done to properly cancel the effects of fringing due to a sapphire coating on the NICMOS 3 array. The coating acts as a Fabry-Perot, producing a non-uniform family of fringes on the spectrally dispersed frames. It is found that dome flats produce a somewhat different fringe pattern, rendering them ineffective at canceling fringes in the observed spectra.

4. Data Reduction Overview

Reduction of the PIFS data is conceptually no harder than reducing any longslit infrared spectral data, as the PIFS output is recorded on the array as eight independent longslit spectra. The sky-subtracted spectra are divided by the normalized main-sequence G-star spectrum, acting both as an atmospheric reference and as the flat-field by the technique described in section 3. Each spectrum is corrected for spatial curvature and spectral curvature, using calibration lamps and OH airglow lines (Oliva & Origlia, 1992) to rectify the spectral domain onto a uniform wavelength grid. The eight spectra are tied together spatially with help of the G-star chopped across all eight slits, as mentioned in section 3. The spectra are then multiplied by a blackbody with the temperature of the G-star used for atmospheric calibration. Each of the eight two-dimensional longslit spectra are then inserted into their proper positions within a datacube. The datacube is more finely gridded in the cross-slit dimension than the number of slits by a factor of four. In this way, the full spatial resolution can be reconstructed provided stable seeing conditions prevail and the dither pattern mentioned in section 3 is followed. Photometric variability from one integration to the next is easily compensated with scaling of the individual spectra to produce a self-consistent spatial profile. The power of integral field spectroscopy in simultaneously acquiring full two-dimensional spatial information is also used to advantage in the data reduction process.

Once the datacube is assembled, pure continuum and pure line images are easily extracted, as are one-dimensional spectra at any point or region within the field. But care must be taken in the interpretation of spectra or in the construction of velocity-resolved line images. The presence of spatial gradients across the various slits induce apparent wavelength offsets with respect to the spatially uniform calibration sources, such as lamp lines and OH lines. Therefore false velocity shifts will be perceived if extracting wavelength bins with respect to the calibration sources. Knowing the local spatial profile of the line emission source, and how this profile is partitioned by the slits is sufficient to reconstruct the apparent velocity shifts. An improved map of line emission gas at a particular velocity can then be constructed, and used, if necessary to iterate until a self-consistent solution is obtained.

5. First Results

The PIFS was first operated on the Palomar 200-inch Telescope in the Fall of 1998. After three observing runs, the instrument has proven itself to be both reliable and scientifically powerful. Example data highlighting the capabilities of the instrument are presented below.

5.1. NGC 6240

The luminous infrared galaxy, NGC 6240 is a well known example of a major galactic merger. The galaxy shows two continuum peaks, or nuclei, separated by $\sim 1\overset{''}{.}5$ at 3.6cm (Colbert et al. 1994). Millimeter-wave studies in CO have indicated the accumulation of cold molecular gas in the region between nuclei (Bryant & Scoville, 1999; Tacconi et al., 1999), in agreement with simulations (e.g., Barnes & Hernquist, 1991) showing the collisional gas leading the stars in coalescing to the central potential. Fabry-Perot imaging of NGC 6240 in the near-infrared by Van der Werf et al. (1993) in three velocity channels showed widespread emission from the 1–0 S(1) vibrational-rotational transition of molecular hydrogen. New data with the PIFS, obtained on 1999 March 27 present a similar picture to the work by Van der Werf et al.

Four five-minute on-source integrations of NGC 6240, with an equal number of sky integrations, produced a datacube around the H_2 1–0 S(1) line at $\lambda_{rest} = 2.12\mu$m. A single raw frame, accompanied by the same frame following sky subtraction is shown in Figure 5, illustrating the arrangement of the eight independent spectra on the array. The unsubtracted OH line emission from the atmosphere is clearly shown. Obvious in the single sky-subtracted frame is extended H_2 emission, differing dramatically in morphology from the continuum source. Also evident is the broad nature of the H_2 line profile, especially contrasted with the 230 km s^{-1} resolution element seen in the OH airglow lines of the raw frame. Figure 6 displays a reconstructed pure continuum image along with total H_2 emission and three velocity bins of the same line feature. The broad nature of the line emission manifests itself in the velocity-resolved line images in that the three images are more similar than different. However, differences do exist, perhaps most notably the shift of the peak H_2 emission from one nucleus to the other as one moves from red to blue.

5.2. 4C 39.37

The $z = 3.22$ FRII radio galaxy, 4C 39.37, was imaged with the PIFS on 1999 March 25. The extent of the object is small enough such that the object can be dithered around within the PIFS field. In this way, 16 five-minute spectral integrations at 2.1μm were taken to capture the [O III] doublet. The resulting spectrum shows definite, nonlinear spatial extension of the line emission, with a large range of velocities seen in the two-dimensional spectra. Figure 7 shows the spatial distribution of the total 0.5007μm line emission, as well as three velocity bins of the same data. The radio axis of the galaxy is oriented horizontally in the figure, which corresponds to the major axis of the line emitting nebula. A clear morphological dependence on velocity is seen, possibly indicative of gas flowing out along the radio axis.

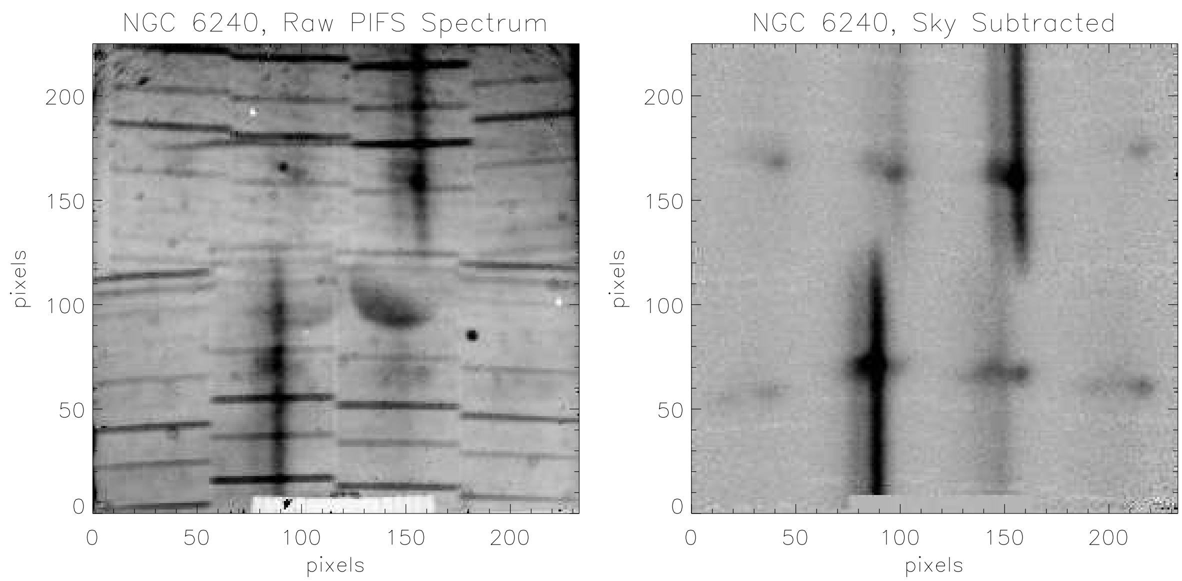

Fig. 5.— PIFS spectra of the H_2 1–0 S(1) line in NGC 6240, representing 5 minutes of on-source integration time in the high resolution mode. The raw frame is displayed at left, and the sky-subtracted frame at right. Wavelength increases outward from the center of the array. The OH airglow lines show the pattern of the slit, which differs from the schematic slit pattern of Figure 1 for reasons discussed in the text. The continuum is clearly visible, marking the central two slits in the rectangular field. The molecular hydrogen emission is immediately seen to show more extent than the continuum, by the fact that line emission appears in all eight slits.

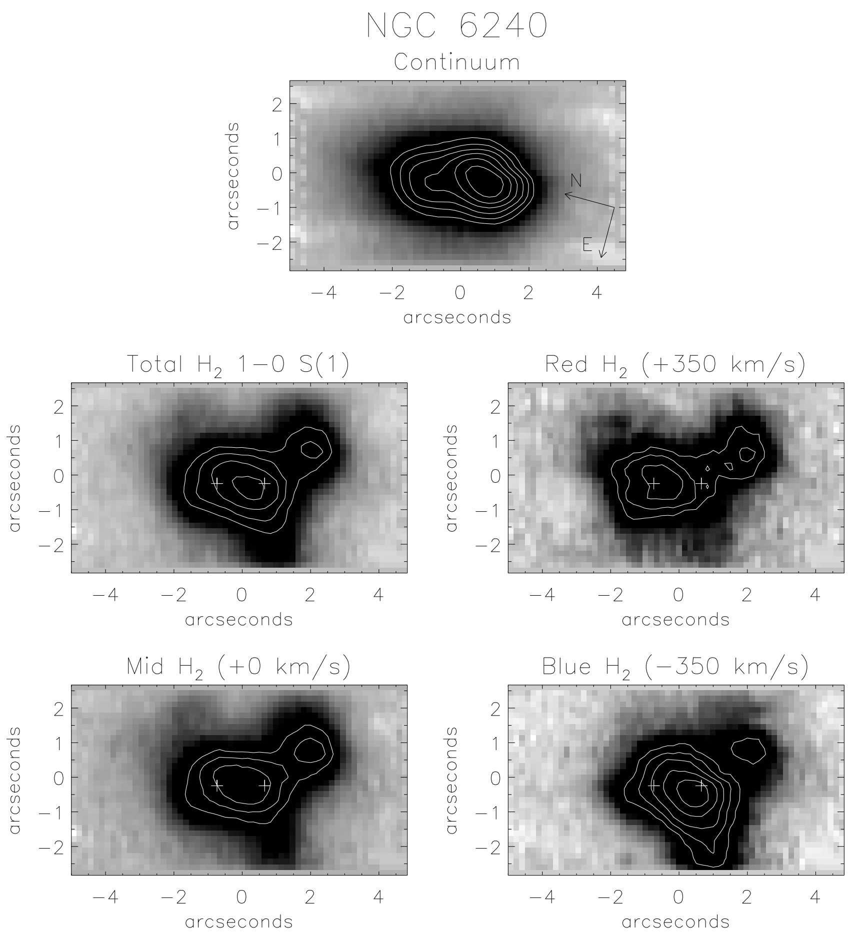

Fig. 6.— Reconstructed images of NGC 6240 from 20 minutes of on-source integration. At top is the pure continuum image, collapsed from the datacube. The two continuum peaks are indicated in subsequent images by crosses. The lower four panels present continuum-subtracted line images of the H_2 1–0 S(1) line, the first showing the total H_2 flux, and the following three panels representing three different velocity bins of the emission line. The velocity bins are 350 km s^{-1} wide, separated by the same amount. The spectral resolution element of the PIFS is 230 km s^{-1}.

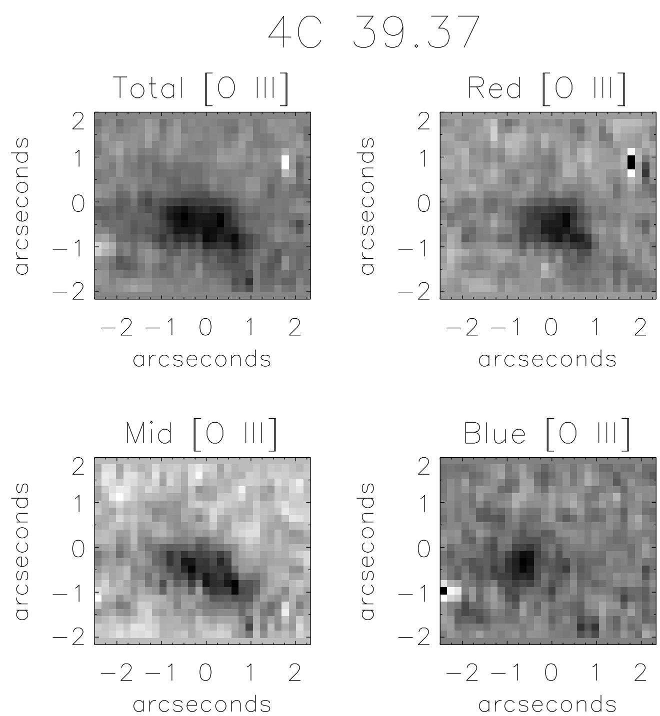

Fig. 7.— PIFS images of [O III] emission in the z=3.22 radio galaxy, 4C 39.37. The data here represent 80 minutes of integration time, with the object dithered within the PIFS field for object-sky pairs. The total line emission, at upper left, shows clear spatial extent, primarily in the horizontal direction, corresponding to the radio axis. Velocity-resolved line images, presented in bins of 350 km s^{-1}, show that the morphology changes as a function of velocity.

6. Summary

We have described the design, construction, and performance of a new cryogenic integral-field spectrograph for near-infrared observations at the 200-inch Hale Telescope. The properties of the spectrograph are summarized here:

1. Operation from 1–2.5μm or 1–5μm with one of two existing 256×256 infrared array cameras.
2. Total field of view of $5''.4\times9''.6$, sliced into eight slits, each $0''.67\times9''.6$in size, with seeing-limited spatial resolution across the entire field of view.
3. Two resolution modes, offering resolutions of $R\approx1300$ and $R\approx600$. Spectral coverage is $\sim$5000 km s^{-1} and $\sim$12000 km s^{-1} for these two modes, respectively.
4. Slit imaging mode for photometric calibration and target acquisition.

The design and construction of the Palomar Integral Field Spectrograph represents part of the thesis work of T. W. Murphy. We thank James Larkin, Robert Knop, and Sean Lin for their roles in developing the longslit spectrograph, which acted as a launching point in the design of the PIFS. Conversations with Gerry Neugebauer helped guide the instrument development. Special thanks to Armando de las Casas, who did a significant portion of the machining work, and to Rick Paniagua, who advised TWM on countless innovative machining techniques, and also made his tool box available. Thanks also goes to Mike Gerfen, Ramon Devera, Richard Borup, Nathaniel White, Terry Scott, Phillip Wood, and Larry Kuntz for their machining contributions to the project. Thanks to Doug Warden for providing odds and ends, and for wiring the motors. Eiichi Egami is thanked for occasionally lending a hand, and for his help with photo-documentation. Diamond fly-cutting of the image slicer optics was performed by Manasota Optics. The PIFS dewar was built by Precision Cryogenics. Don Loomis figured the fused silica optics. Infrared Optical Products provided the CaF_2 windows, and the gratings were replicated by Richardson Grating Lab. Thanks to telescope night assistants, Rick Burruss, Karl Dunscombe, and Jean Mueller for their skillful manipulation of the telescope. We are also grateful for the efforts of Mike Doyle, Dave Tenant, Steven Kunsman, John Henning, and the rest of the Palomar staff, whose efforts promoted problem free integration of the PIFS into the existing infrastructure. Lee Armus accompanied some of the observations presented here. Funding for the PIFS was provided by the National Science Foundation, and by grants from the W.M. Hurt Foundation and Caltech. TWM is supported by the NASA Graduate Student Researcher Program.

REFERENCES

Barnes, J. E., & Hernquist, L. 1991, ApJ, 370,L65

Bryant, P., & Scoville, N. Z. 1999, to appear in June AJ

Colbert, E. J. M., Wilson, A. S., & Bland-Hawthorn, J. 1994, ApJ, 436, 89

Larkin, J. E., Knop, R. A., Lin, S., Matthews, K., and Soifer, B.T. 1996, PASP, 108, 211

Oliva, E., & Origlia, L. 1992, A&A, 254, 466

Tacconi, L. J., Genzel, R., Tecza, M., Gallimore, J. F., Downes, D., and Scoville, N. Z. 1999, Ap.J., submitted.

Van der Werf, P. P., et al. 1993, ApJ, 405, 522

Weitzel, L., Krabbe, A., Kroker, H., Thatte, N., Tacconi-Garman, L. E., Cameron, M., and Genzel, R. 1996 A&AS, 119, 531

This preprint was prepared with the AAS LaTeX macros v4.0.